Combining Front Propagation with Shape Knowledge for Accurate Curvilinear Modelling

Rongxin Li and Sébastien Ourselin

BioMedIA Lab
CSIRO ICT Centre
Cnr Vimiera & Pembroke Rd, Marsfield NSW 2122, Australia
{Ron.Li, Sebastien.Ourselin}@csiro.au
http://www.tip.csiro.au

Abstract. In this paper, we propose an approach to accurately modelling tubular, anatomical structures as curvilinear entities. Current optimal path and centerline extraction techniques are either prone to introducing spurious tortuosity, or unable to consistently avoid taking shortcuts at high curvature positions. These problems not only affect spatial appreciation of the structure but may also significantly impact the accuracy of length, angle and tortuosity measurements. Our approach overcomes the above deficiencies through the combination of a front propagation method and a model in which *a priori* shape knowledge is embedded. This approach is designed to be used in endovascular and neurological surgical planning. The efficacy of our method is demonstrated using synthetic and clinical data.

1 Introduction

In neurosurgery or endovascular surgery, a precise understanding of the patient's vessel system is of fundamental importance. Accurate curvilinear modelling of anatomical tubular structures is likely to become a crucial part of computer-assisted surgery planning.

With existing centreline extraction algorithms, a high level of accuracy of the curvilinear model cannot be guaranteed. A common drawback of the existing techniques is that they are not sufficiently resistant to neighbourhood interference. This may significantly affect the accuracy of any length and tortuosity measurements based on such models.

In this paper, we address these problems using a combination of wave-propagation and shape constraints using an adaptive tubular deformable model.

This paper is structured as follows: we review the relevant literature in Section 2, we detail the different steps of our new algorithm in Section 3. In Section 4, we demonstrate the accuracy of our method using Magnetic Resonance Angiography (MRA) of the brain.

R.E. Ellis and T.M. Peters (Eds.): MICCAI 2003, LNCS 2879, pp. 66–74, 2003.

2 A Brief Review of Existing Methods

We define *accurate curvilinear modelling* in the following way: an accurate curvilinear model (ACM) of a tubular entity is an abstraction of the object that retains only those geometric properties that are essential to length, angle and tortuosity measurements. It excludes all potentially interfering details such as width, width change (*e.g.* aneurysms) and branching. This exclusion is a major distinction from other, similar or related forms of representation, such as the medial axis or M-Rep [2,13].

Due to the close relationship of curvilinear models to medial axes and centerlines, we review methods for extracting centerlines (or medial axes) even though in many situations they may not be suitable for constructing an ACM.

A classic method for extracting medial axis is the skeletonisation technique. This is often achieved by topology-preserving thinning after region growing [12]. In a more recent development, ordered region growing is used, followed by pruning [20].

Alternatively, voxels in the middle of a curvilinear structure can be located by convolving the image with appropriate Gaussian kernels. On certain scales (variance of the Gaussian), a ridge appears in the middle of a tubular structure (e.g. [1]). A model-based, scale-space filtering approach has also been proposed by several authors [8,14,9]. The centerline is located by detecting optimal responses derived from Hessian matrices at a range of scales of interest. This class of algorithms produce good results but problems may occur at junctions or tangent vessels.

Direct tracking from a seed point has also been used to extract the optimal path. From a given point, the most likely local orientation of the vessel can be searched or predicted [19,10]. Further iterative search or prediction and centering is carried out until the end position is reached. The fidelity of the model to the "true" centerline thus extracted depends heavily on the centering algorithm.

Graph-search principles can be used as well to calculate a Minimal Cost Path (MCP). To achieve this, Dijkstra's algorithm has proved to be the most efficient and widely used [7]. However, this algorithm can fail because of the ambiguity that arises from restricting the calculation of costs to the discrete grid points.

A recent approach proposed by Deschamps *et al* incorporates multiple improvements over the standard Fast Marching Method (FMM) [15]. It includes a technique of using multiple passes of FMM (from different initial positions) to centre the track [6,18]. This technique corrects the inherent tendency of MCP algortihms to discourage large curvatures. However, it can introduce artificial tortuosity under certain circumstances (see Figure 1). While it is possible to smooth the track by adding a relatively large constant into the cost integral, such smoothing tends to cancel out the work performed by the path centering technique, especially at high curvature positions. This is a dilemna. It is our belief that only through the use of *a priori* knowledge can this issue be satisfactorally resolved.

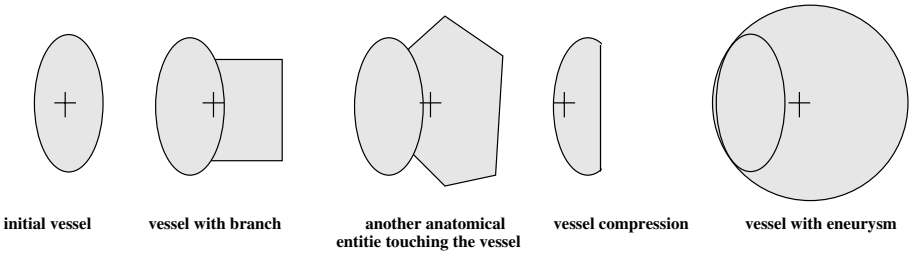

Fig. 1. *Using a non-model based detection method, interference from foreign objects may cause a shift in the detected center from its "true" position. Note that the main structure is not perfectly circular but elliptical, which makes it even less resistant to outside interference.*

3 Description of the Method

The method presented here for accurate curvilinear modelling uses *a priori* shape knowledge embedded in a deformable model. In addition, it also embodies front propagation. We use a modified tubular deformable model to implement the constraints. A distance field is first constructed and then uniformly thresholded to obtain suitable propagation channels. A propagation map is then constructed from a start point using FMM, and then backtracked when the end is reached to generate the Minimal Cost Path.

At each point on the MCP, the original data is resampled in planes perpendicular to the local orientation of the MCP. A deformable tubular model is constructed inside the resampled data and allowed to deform so that it recovers the object of interest. Towards the end of the deformation, an adaptive deflation force replaces the original inflation force. Finally, the curvilinear model is obtained by extracting the spine of the tubular model and transforming it back into the coordinates of the original data. This process ensures that rapid symmetric changes, such as a sharp turns, are not lessened while many asymmetric changes, such as a branching event or aneurysms, can be removed to a large extent. In addition, deforming the model in the transformed data domain vastly simplifies the computation, making it efficient.

3.1 Distance Field Computation

Instead of being used to extract the centerline through topology-preserving thinning or ridge enhancement as reviewed in Section 1, distance transforms are used in our method as a pre-processing step for larger structures to reduce the widths of propagation channels. Doing so achieves two purposes. Firstly, it helps the tubular model in the next stage to remain faithful to the structure of interest (especially at high curvature parts of the structure) and promotes faster convergence of the deformation of the model. This is because better initialization for the tubular model can be achieved with narrower propagation channels

relative to the axial curvature, and with those channels well inside the structure of interest. This will become apparent in Section 3.3.

Secondly, higher efficiency can be achieved by reducing the size of propagation channels. Apart from the reason shown in [6], another, perhaps more important, rationale is that it reduces the extent of branching and neighbourhood touching - two major causes of propagation leakage - in much the same way as erosion.

This pre-processing is performed by first thresholding the image, and then computing a distance map using a chamfer algorithm [11]. Once the end points and are selected, a connected-component analysis is performed to determine the local peaks in their neighbourhoods in the distance map. The distance map is thresholded if the values at those peaks exceed a target value.

By using the chamfer transform, we avoid the need to administer multiple passes of FMM, as proposed by Deschamps *et al* and the additional system complexity that it brings [6]. Although the resultant distances are not exactly Euclidean, this does not affect our results. This is because only the order of distances, rather than the distance values per se, are of interest to our method. Using any of the common chamfer matrices [3], that order is preserved on any size of grids for CT or MRI scans.

3.2 Minimal Cost Paths, Front Propagation, and Fast Marching

The MCP approach is both effective and robust for extracting curvilinear structures such as vasculature and the colon. It is robust to many conditions such as vessel stenosis, partial volume effects and noise. Unfortunately, minimizing the path integral of a cost function is an intractable NP-complete problem.

Simulated front propagation has recently emerged as a desirable approach to finding the MCP. Not only is it efficient, but it can also give sub-grid accuracy.

A commonly used method for efficiently tracking the propagating front is the FMM proposed by Sethian [15,16]. Provided that the speed of the propagation is monotonic, interface arrival times are governed by the Eikonal equation $|\nabla T|F = 1$, where T is the arrival time of the front, and F its speed. The front speed is defined as:

$$F = \frac{G_\sigma * I}{\max(G_\sigma * I)} + \alpha,$$

where I is the image, G_σ is a Gaussian kernel and α is a small constant.

Efficient entropy-satisfying numerical methods have been developed by Sethian and his associates based on the Hyperbolic Conservation Laws. After a forward marching phase, backtracking from anywhere in the field in the direction of steepest decent will reach the origin of the propagation. Thus, from a pre-determined end point, a minimal cost path can be found via wave propagation simulated using FMM.

3.3 *A priori* Shape Knowledge

The safest way to avoid spurious tortuosity being introduced, while ensuring that any real tortuosity is not under represented by the model, is to filter out

any bumps, branches or foreign objects in the neighbourhood in a pre-processing stage. However, to do so reliably, one needs to apply *a priori* knowledge about the desired and irrelevant structures.

A tubular shape model. We use an active surface model as a vehicle to carry knowledge about the structure of interest. The basic mechanisms of the model is described in [17,5]. Unlike previous usages, however, the deformation of our model only takes place in a tranformed image.

The knowledge is embedded both in the mesh structure and the internal forces of the model. Specifically, the combination of the intra-ring forces (see below) and the inflation force alone favours such a resultant tubular model that each cross-secontional ring is of a nearly constant area. The inter-ring forces help enforce this. However, in the present application the inter-ring forces play a secondary role. The internal forces can be designed so that the constant area favoured by the model approximately corresponds to that of the structure being modeled. The use of an adaptive deflation force (see below) near the end of the deformation provides additional assurance. The image force localizes the model.

Model evolution in the transformed image domain. At each point on the MCP, the original data are thresholded and resampled in planes perpendicular to the local orientation of the MCP, and stacked up to form a new, transformed data volume. An initial thin tube is constructed in the middle of the new data and allowed to evolve to minimize the following "energy" functional E of the model in a space of permissible deformations [17,5]:

$$E(v) = \int_{\Omega} w_{10} \left| \frac{\partial v}{\partial s} \right|^2 + w_{01} \left| \frac{\partial v}{\partial r} \right|^2 + w_{11} \left| \frac{\partial^2 v}{\partial s \partial r} \right|^2 + w_{20} \left| \frac{\partial^2 v}{\partial s^2} \right|^2 + w_{02} \left| \frac{\partial^2 v}{\partial r^2} \right|^2 + P[v(s,r)] \; dsdr$$

where v is a parametric surface, and s and r are the parameterisation in the cross-sectional-tangential and axial directions respectively. The potential $P(v)$ can be defined as $-\|\nabla I(v)\|$, where I is the image. Used in our model, the coefficients w_{10} and w_{20} encode the strengths of the intra-ring forces mentioned above, while w_{01} and w_{02} represent those of the inter-ring forces. w_{11} is associated with a combination of intra and inter-ring forces. An inflation force is also used throughout the entire process.

After the model converges at a local energy minimum, the evolution process is repeated three times, each time using the previous result for the initialisation (the first two rounds after shrinking the tube). This improves the deformable model's initialisation at places with significant curvature.

In the final round of the iterative deformation, the resultant model from the previous round is not shrunken prior to the initialisation, but an additional adaptive deflation force is used. Similar to the adaptive forces proposed in other research (*e.g.* [4]), this force is almost inversely proportional to the magnitude

of the local gradient. This force is used because the area targeted by the balance between the intra-ring and inflation forces may not always be precise. To avoid the need to use strong forces in the axial direction of the tube in such a situation, we use adaptive deflation to reverse any "leakage" because of gradient deficiencies. Finally, the medial axis is transformed back to the coordinate system of the original data to form the ACM.

4 Results

We demonstrate that our approach can produce ACMs in two situations, respectively representing the two opposite aspects of the dilemma mentioned in Section 2. The same set of model parameters is used for both of the situations.

Synthetic data. Our approach is applied to a situation where there is significant potential interference in the neighbourhood of a tubular structure. As shown in Figure 2, the elliptical shape of the cross-section of the main structure makes it less resistant to outside interference. Our result, specifically the ACM shown inside the 3D visualisation, is not affected at all by the bulge in the middle of the target structure.

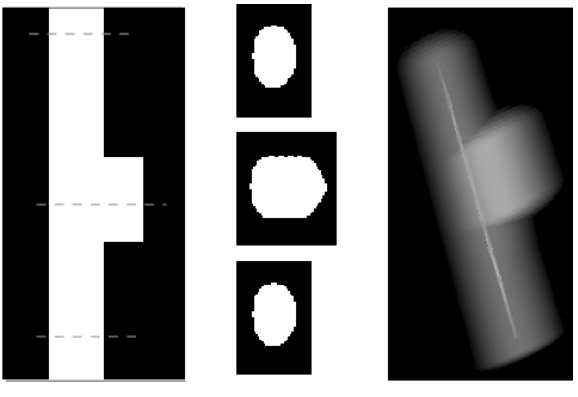

Fig. 2. *Form left to right: tubular structure with outside interference; 3 different cross-section of the tubular structure; ACM with a 3D visualiation of the tubular structure.*

Magnetic Resonance Angiography. We illustrate our method with one MRA image with a resolution of $284 \times 512 \times 112$ ($0.48mm \times 0.48 \times 0.83mm$). We computed the curvilinear model of the internal carotids. This can be a prepocessing step for a neurosurgey planning. The initial data and the results for the two internal carotids are shown in Figure 3. In the bottom left panel of Figure 3 we compare the MCP (dotted line) with the curvilinear model (solid

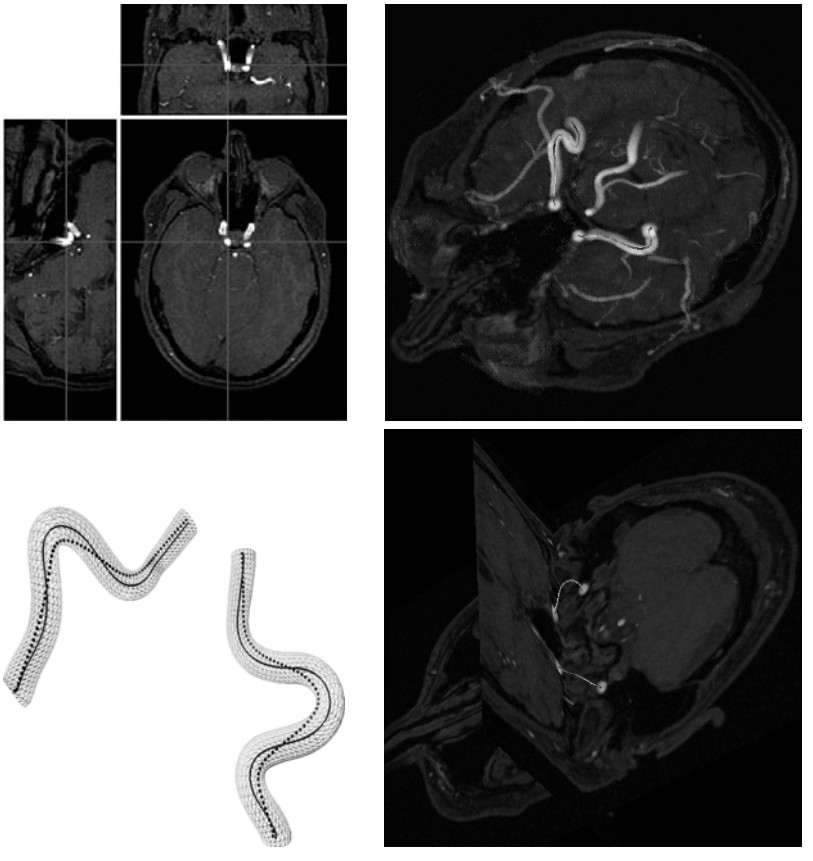

Fig. 3. *Curivilinear models of the internal carotids. Top left: axial, sagital and coronal view of the original MRA; Top right: MIP of the vessels with the ACM superimposed; bottom left: comparison of the MCP (dotted line) with the ACM (solid line); bottom right: ACM with two cutting plans of the MRA superimposed.*

line). In the top right panel the carotids are visualised using Maximum Intensity Projection (MIP), along with their ACMs.

5 Discussion and Conclusion

We argue that to guarantee a high degree of accuracy in length, angle and tortuositiy measurements for surgical (*e.g.* endovascular) planning purposes, potentially interfering irrelevancies should be filtered out before extracting a model suitable for the measurements. Furthermore, we believe that such filtering must involve some *a priori* knowledge regarding the structures concerned. A particular term, curvilinear modelling, has been used to describe procedures that satisfy those criteria.

In this paper, we have described one particular method for accurate curvilinear modelling. We haved demonstrated that it is resistant to introducing spurious curvatures (those that are not due to any change in the local orientation of the object of interest), while faithfully reproducing "real" high curvatures (those that are actually part of the object in question).

Further improvements. A deformable tubular model and a front propagation approach are the two main elements used in the filtering and the extraction. However, it may be worth investigating modifications to, or even replacement of, either of those. For example, in addition to the implicit constant area constraint, explicitly incorporating the following adaptivity in the intra-ring forces might help improve the robustness of this approach:

$$w_{01}(i, i+1) = \alpha \left[\max(a_i, a_{i+1}) - \min(a_i, a_{i+1})\right] + \beta,$$

where a_i and a_{i+1} are the areas of two successive rings of the model, with α and β two parameters to tune.

Acknowledgments. The authors would like to thank the Neurological Service of Henri Mondor Hospital (Créteil, France) for the MRA image. We would also like to thank Neil Killeen and Bhautik Joshi for proofreading of this article.

References

1. S. Aylward and E. Bullitt. Initialization, Noise, Singularities and Scale in Height Ridge Traversal for Tubular Object Centerline Extraction. *IEEE TMI*, 21(2):61–75, 2002.
2. H. Blum. A transformation for extracting new descriptors of shape. In D. Wathen, editor, *Models for the Perception of Speech and Visual Form*, pages 363–380. MIT Press, Cambridge MA, 1967.
3. G. Borgefors. Distance transformations in arbitrary dimensions. *Comput. Vision Graphics Image Process*, 27:321–345, 1984.
4. V. Chalana, W. Costa, and Y. Kim. Integrating region growing and edge detection using regularization. In *SPIE*, volume 2434, pages 262–271, 1995.
5. L. Cohen and I. Cohen. Finite-Element Methods for Active Contour Models and Balloons for 2-D and 3-D Images. *IEEE PAMI*, 15(11):1131–1147, November 1993.
6. T. Deschamps and L.D. Cohen. Fast extraction of minimal path in 3D images and applications to virtual endoscopy. *Medical Image Analysis*, 5:281–299, 2001.
7. Edsger W. Dijkstra. A note on two problems in connexion with graphs. *Numerische Mathematik*, 1:269–271, 1959.
8. A.F. Frangi, W.J. Niessen, K. Vinken, and M.A. Viergever. Multi-scale vessel enhancement filtering. . In *MICCAI'98*, volume 1496 of *Lecture Notes in Computer Science*, pages 130–137, Cambridge (USA), October 1998. Springer.
9. K. Krissian, G. Malandain, N. Ayache, R. Vaillant, and Y. Trousset. Model-Based Detection of Tubular Structures in 3D Images. *CVIU*, 80:130–171, 2000.
10. R. Li, S. Brown, L. Wilson, J. Young, and S. Luo. Progressively Refined Patient-Specific Vessel System Models from Generic Representations. In *DICTA'02*, pages 184–189, Melbourne, Australia, October 2001.

11. G Lohmann. *Volumetric Image Analysis*. Wiley, 1998.
12. N. Nikolaidis and I. Pitas. *3-D Image Processing Algorithms*. John Wiley, 2001.
13. S.M. Pizer, A.L. Thall, and D.T. Chen. M-reps: A New Object Representation for Graphics. Technical Report TR99-030, Uni. N. Carolina, Chapel Hill, Sep. 1999.
14. Y. Sato, S. Nakajima, N. Shiraga, H. Atsumi, S. Yoshida, T. Koller, G. Gerig, and R. Kikinis. Three-Dimensional Multi-Scale Line Filter for Segmentation and Visualization of Curvilinear Structures in Medical Images. *Medical Image Analysis*, 2(2):143–168, 1998.
15. J.A. Sethian. A fast marching level set method for monotonically advancing fronts. *Proc. of the National Academy of Sciences of the USA*, 93(4):1591–1595, Feb 1996.
16. J.A. Sethian. *Level set methods: Evolving interfaces in geometry, fluid mechanics, computer vision, and materials science*. Number 3 in Cambridge monographs on applied and computational mathematics. Cambridge University Press, 1999.
17. D. Terzopoulos, A. Witkin, and M. Kass. Constraints on deformable models: Recovering 3D shape and nonrigid motion. *Artif. Int.*, 36(1):91–123, 1988.
18. R. Truyen, T. Deschamps, and L.D. Cohen. Clinical Evaluation of an Automatic Path Tracker for Virtual Colonoscopy. In *MICCAI'01*, pages 169–176, Utrecht, The Netherlands, October 2001.
19. O. Wink, W.J. Niessen, and Viergever M. Fast Delineation and Visualization of Vessels in 3-D Angiographic Images. *IEEE TMI*, 19(4):337–346, 2000.
20. P.J. Yim, P.L. Choyke, and R.M. Summers. Gray-Scale Skeletonisation of Small Vessels in Magnetic Resonance Angiography. *IEEE TMI*, 19(6):568–576, 2000.